ACADEMIC PRESS

Available online at www.sciencedirect.com
SCIENCE DIRECT®

Journal of Catalysis 218 (2003) 54–66

JOURNAL OF CATALYSIS

www.elsevier.com/locate/jcat

A substrate-versatile catalyst for the selective oxidation of light alkanes II. Catalyst characterization

Christopher J. Dillon,[a] Joseph H. Holles,[a] Robert J. Davis,[b] Jay A. Labinger,[c] and Mark E. Davis [a,*]

[a] *Chemical Engineering, California Institute of Technology, Pasadena, CA 91125, USA*
[b] *Department of Chemical Engineering, University of Virginia, Charlottesville, VA 22904, USA*
[c] *Beckman Institute, California Institute of Technology, Pasadena, CA 91125, USA*

Received 17 September 2002; revised 11 December 2002; accepted 16 December 2002

Abstract

A highly active and selective catalyst for light alkane oxidation that is composed of a pyridine salt of niobium-exchanged molybdo(vanado)phosphoric acid ($NbPMo_{11}$(V)pyr) is characterized using TGA–DSC, ^{31}P MAS NMR, and in situ powder XRD, XAS, and XPS. The presence of both niobium and pyridinium species strongly influences structural and redox properties of the polyoxometalate. Activation of the catalyst by heating to 420 °C in an inert atmosphere removes all of the organic species present in the solid, and structural rearrangement of the starting heteropolyanion occurs at 420 °C as evidenced by ^{31}P NMR and EXAFS. XRD shows that activated $NbPMo_{11}$Vpyr consisted of a mostly amorphous molybdenum oxide phase, the formation of which is strongly related to the composition of the catalyst. The presence of niobium as an exchange cation $(NbO)^{3+}$ or a framework atom $PMo_{11}NbO_{40}^{4-}$ in the Keggin unit is verified by EXAFS for $NbPMo_{11}$Vpyr and (VO)PMo_{11}Nbpyr, respectively. During activation of either catalyst, niobyl species migrate and most likely coordinate to molybdenum oxide octahedra. Comparison of near-edge electronic spectra (XANES) for as-made $NbPMo_{11}$Vpyr and after activation that removes the pyridinium ions suggests reduction of Mo^{6+} to Mo^{5+} and Nb^{5+} to Nb^{4+}. Under hydrocarbon-rich reaction mixtures molybdenum and niobium remain in their reduced state.

Keywords: Heterogeneous catalysis; Alkane oxidation; Polyoxometalate catalysts; In situ; Characterization; X-ray absorption spectroscopy; Molybdenum oxide

1. Introduction

The design and synthesis of transition metal oxide catalysts are currently a main focus for both industrial and academic laboratories who are pursuing the goal of selective alkane oxidation [1]. Catalytic oxidation of light alkanes is attractive from an industrial perspective due to the economic implications of using a globally abundant raw material. Isopolyoxometalates and heteropolyoxometalates can be designed at the molecular level and used as building blocks to prepare novel oxide materials that can be highly definable and tunable catalysts [2].

The self-organization of polyoxometalates has been shown to be a promising strategy for catalyst synthesis. Much attention has been paid to hydrothermal synthesis as a technique for preparing oxide catalysts containing molybdenum and vanadium, often with niobium and tellurium [3–5]. These materials are generally formed through the self-organization of Anderson-type heteropolyanions ($TeO_6Mo_6O_{18}^{6-}$) and vanadyl (VO^{2+}) or niobyl (NbO^{3+}) cations. A procedure for synthesizing mixed-metal oxides such as $MoVTeNbO_x$ has been developed by Mitsubishi Chemical Corporation through the self-assembly of paramolybdate and telluric acid, and incorporation of vanadate and niobyl precursors in aqueous solution followed by a complex redox process at elevated temperatures [6]. $MoVNbTe(Sb)O_x$ composite oxide catalysts can also be prepared through the reductive linkage of polyoxometalates under mild conditions using reducing agents such as hydrazine and hydroxylamine [7]. Both these mixed oxides have been found to be attractive oxidation catalysts.

* Corresponding author.
E-mail address: mdavis@cheme.caltech.edu (M.E. Davis).

0021-9517/03/$ – see front matter
doi:10.1016/S0021-9517(03)00009-5

It has been proposed that polyoxometalates exist in a structure hierarchy [8]. Design at the atomic level can be achieved through heteroatom selection and substitution of framework atoms of the heteropolyanion (primary structure). Perhaps the most encountered catalysts are vanadium-substituted phosphomolybdates [9], though iron and copper have also been shown to be potential framework atoms for oxidation catalysts [10,11]. The three-dimensional network (secondary structure) allows strategic design on the molecular level: the structure offers the possibility of incorporating countercations and additional molecules (as linker molecules) that strongly influence catalytic properties [12]. Particle size and pore structure can be varied.

The ability to define and tune polyoxometalate catalysts and to produce catalytic activity allows for a better understanding of structure-activity relationships in this class of catalytic materials. In Part I, the reactivity of niobium and pyridine-exchanged phospho(vanado)molybdate catalysts were reported for the oxidation of *n*-butane and propane [13]. Here, the characterization of the structural and electronic properties of this new catalyst system is presented in an attempt to understand and rationalize the extraordinary reactivity.

2. Experimental section

The catalysts used in this work were prepared as described in the preceding paper [13]. Henceforth, phosphomolybdic acid, phosphovanadomolybdic acid, niobium-exchanged phosphovanadomolybdic acid, niobium and pyridine-exchanged phosphovanadomolybdic acid, and vanadyl and pyridine-exchanged phosphoniobomolybdic acid will be denoted as PMo_{12}, $PMo_{11}V$, $NbPMo_{11}V$, $NbPMo_{11}V$pyr, and (VO)PMo_{11}Nbpyr, respectively. Bulk elemental analyses were performed by Galbraith Laboratories Inc. (Knoxville TN).

Simultaneous thermogravimetric analyses (TGA) and differential scanning calorimetry (DSC) were carried out on a Netzsch STA 449C Jupiter spectrometer. The samples were mounted in platinum crucibles and heated at 10 °C/min to 700 °C in a stream of flowing helium. Infrared spectra were collected on a Nicolet Nexus 470 FTIR spectrometer using KBr wafers (1 wt% solid in KBr). Nitrogen adsorption isotherms were obtained at 77 K using an Omnisorp 100 apparatus.

^{31}P solid-state NMR measurements were performed on a Bruker Avance 500 spectrometer using magic-angle spinning. The spectra were acquired at 202.5 MHz with a spinning rate of 10 kHz and a delay time of 3 s. H_3PO_4 (85% solution) was used as an external reference. Samples were heated under flowing dry helium and transferred to the NMR rotor in a glove box to avoid any exposure to moisture.

Powder X-ray diffraction (XRD) was carried out on a Scintag Model XDS 2000 diffractometer equipped with a liquid nitrogen-cooled germanium solid-state detector and using Cu-K_α radiation. For high-temperature measurements under flowing nitrogen, samples were mounted as thin films on a platinum-rhodium alloy sample mount/strip heater enclosed in an in situ cell operated by a Micristar temperature control unit. Sample cell volume was 800 mL with a nitrogen flow rate of 60 mL min^{-1}. Sample heating rate was 5 °C min^{-1} with a 15 min hold time before scanning. Scan rate was 1° min^{-1}.

The X-ray absorption spectra (XAS) from the Nb K edge (18,986 eV) and the Mo K edge (20,000 eV) were recorded in transmission mode on beamline X18B at the National Synchrotron Lightsource, Brookhaven National Laboratory (Upton NY). In addition to examining the catalysts, XAS from the following standards were obtained: Nb_2O_5 (Aldrich), NbO_2 (Aldrich), NbO (Aldrich), MoO_3 (Alfa), MoO_2 (Aldrich), MoS_2 (Alfa), and Nb and Mo foils (Goodfellow). The storage ring operated with an electron energy of 2.8 GeV with beam currents ranging from 150 to 250 mA. During XAS measurement, appropriate metal foils were placed between the second and the third ionization chambers as energy calibration standards. For operation at both the Nb and the Mo K edges, the first chamber was filled with a mixture of nitrogen and argon (50/50) and the second and third chambers were filled with argon alone. Sample powders were diluted in boron nitride (Alfa), pressed into self-supporting wafers, and placed in an in situ sample cell capable of both heating and cooling the wafer in controlled atmospheres. The loading of sample in boron nitride was adjusted to obtain $\Delta\mu x = 0.33$ for Nb and 1.0 for Mo in order to maximize the ratio of signal to noise. The sample cell consisted of a stainless-steel chamber with water-cooled Kapton windows and a copper sample holder that contained electrical cartridge heaters. The cell was purged with helium for room temperature scans. The cell was then heated at 3 °C min^{-1} to obtain spectra at 200, 350, and 420 °C, before cooling to 380 °C and exposure to a reaction mixture of 16:8:16:20 mL min^{-1} of *n*-butane (99% Aldrich):oxygen:helium:steam. The reactant gases were introduced to the sample cell using electronic mass flow controllers via a stainless-steel line next to the sample wafer. At least three X-ray absorption spectra were collected at each temperature. The data were processed using WinXAS 97 [14]. The raw EXAFS data were extracted from the absorption spectra and normalized by dividing the absorption spectra by the postedge polynomial. Postedge background subtraction was done with a cubic spline and 6 knots. The EXAFS were k^3-weighted before additional processing. For the molybdenum data, the transformed range was 4.9 to 16.7 Å^{-1}. The radial structure functions were back-transformed over the range 2.65 to 3.66 Å and fitted to a MoS_2 standard having the first Mo–Mo shell at 3.15 Å and a coordination number of 6 [15]. Niobium analysis was performed over the range of 4.4 to 13 Å^{-1}. For Nb–O, the back-transform range was 1.23–1.91 Å that was fitted to a NbO standard having an interatomic distance of 2.105 Å with coordination number of 4. The back-

transform range for Nb–Mo was 2.38–3.44 Å that was fitted to NbO having the first Nb–Nb shell at 2.987 Å with a coordination number of 8 [16]. The Nb–O and Nb–Mo shells were fitted separately. Interatomic distance, coordination number, Debye–Waller factor, and edge energy shift were all free floating for each shell fitted. Uncertainties associated with the structural parameters are similar as those generally accepted for the EXAFS technique, ±20% for N (coordination number), ±10% for $\Delta\sigma^2$ (change in Debye–Waller factor), and ±0.01 Å for R (interatomic distance).

Photoelectron spectroscopy measurements (XPS) were carried out on a Surface Science Instruments SSX-100 XPS spectrometer. Small amounts (<100 mg) of each sample were pressed into 99.99% indium foil. The pellets were analyzed with a ∼600 μm spot size microfocused Al-K_α X-ray source and a measured resolution of 0.069 eV. An in situ treatment system was employed to ramp the temperature for 3 to 4 h to 420 °C and held for 5 h in 5 Torr of flowing helium. The sample was allowed to cool overnight in flowing helium before the spectra were obtained. All transfers were performed under UHV conditions in around 15 min.

3. Results

3.1. Thermogravimetric analysis and differential scanning calorimetry (TGA–DSC)

TGA–DSC analyses of $PMo_{11}V$ and $NbPMo_{11}Vpyr$ are presented in Figs. 1 and 2. The measurements were acquired while heating the catalyst from room temperature to 700 °C under flowing helium. A weight loss is observed for $PMo_{11}V$ from room temperature to 200 °C that is attributed to the desorption of crystallization water (10 water molecules per Keggin unit) that is incorporated in the secondary structure of the heteropolyacid during synthesis. At 430 °C an exothermic phase transition is observed from the DSC trace

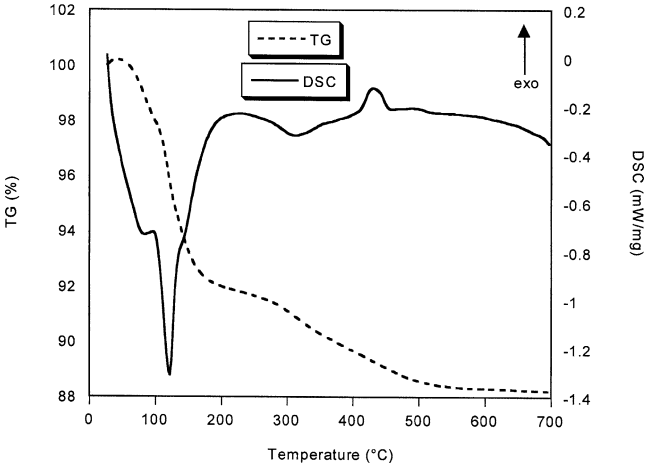

Fig. 1. TGA–DSC of $PMo_{11}V$ under helium from room temperature to 700 °C.

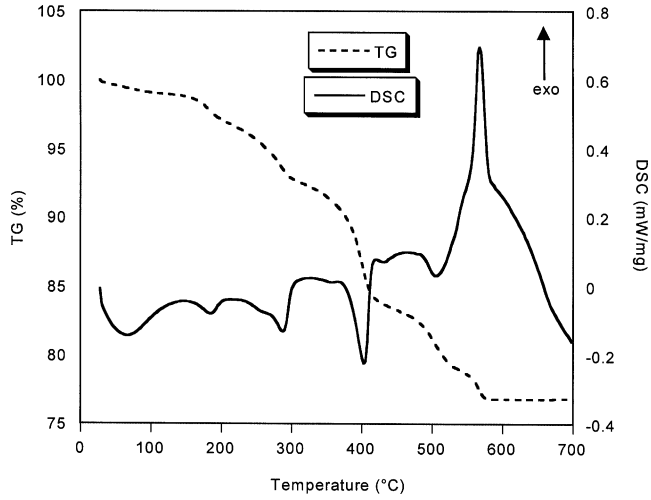

Fig. 2. TGA–DSC of $NbPMo_{11}Vpyr$ under helium from room temperature to 700 °C.

that is identified from powder X-ray diffraction as originating from a transformation into molybdenum trioxide MoO_3. In comparison to $PMo_{11}V$, less water of crystallization is associated with $NbPMo_{11}Vpyr$ ($1H_2O$/Keggin); the water has likely been replaced by pyridine that is incorporated in the secondary structure during synthesis. This "occluded" pyridine is observed to desorb around 200 and 290 °C. The major weight loss at around 400 °C can be attributed to desorption of pyridinium ions that partially balance the negative charge on the heteropolyanion. By 420 °C complete removal of pyridine species is achieved as evidenced by infrared spectroscopy. Further weight loss is observed at higher temperatures and is attributable to removal of oxygen from the polyoxometalate resulting in decomposition and reduction to molybdenum dioxide (MoO_2) at 565 °C as identified by powder XRD.

Table 1 gives the elemental analysis of PMo_{12}, $NbPMo_{12}$, and $NbPMo_{12}pyr$. An excellent agreement is observed between the measured bulk composition (ICP-MS) and the composition used in the synthesis. For $NbPMo_{12}pyr$ it is calculated from bulk elemental analysis that there are 3.61 mol of pyridine species present (pyridine or pyridinium) per mole of heteropolyanion based on the nitrogen composition; 5.01 carbon atoms per nitrogen were found, suggesting no oxalic acid remained in the material after drying. Niobium is likely associated with the heteropolyanion as an oxocation (NbO^{3+}), considering the niobium oxalate precursor and EXAFS data. Niobium will contribute a positive charge of 0.7 ($= 3 \times 0.22$) to balance the heteropolyanion charge of −3. The remaining negative charge of 2.3 is balanced by pyridinium species resulting in a pyridinium/pyridine ratio of 1.8. TGA analysis was performed using 29.0 mg (14 μmol) of $NbPMo_{12}pyr$, which 31 μmol of pyridinium species (2.5 mg) should be associated with if the charge balance is correct. Indeed, a decrease of 2.3 mg is observed over the range 380 to 420 °C by TGA, confirming that this weight loss corresponds to the desorption of all pyridinium species.

Table 1
Calculated catalyst elemental composition

Catalyst	Nb/P/Mo Synthesis composition	Nb/P/Mo/C/H/N Bulk composition (ICP-MS)	Nb/P/Mo Surface composition (XPS)	
			As-made	Act. 420 °C
PMo_{12}	−/1/12	–	−/1/9.14	−/1/3.45
$NbPMo_{12}$	0.25/1/12	0.23/1/12.23/ − / − /−	0.14/1/9.00	0.09/1/5.16
$NbPMo_{12}$pyr	0.25/1/12	0.22/1/11.99/18.06/24.12/3.61	0.29/1/9.36	0.17/1/7.75

3.2. ^{31}P NMR MAS spectroscopy

^{31}P NMR is a useful technique for studying the integrity of the primary structure of phosphorus-containing polyoxometalates. The ^{31}P NMR chemical shift is very sensitive to thermal treatment. In order to investigate the structural stability of $NbPMo_{11}$Vpyr during activation, ^{31}P MAS NMR spectra were recorded at various temperatures during the heating from room temperature to 420 °C under a flowing inert atmosphere. The spectra are given in Fig. 3.

The ^{31}P MAS NMR of $NbPMo_{11}$Vpyr at room temperature exhibits a single narrow resonance at δ −4.3 ppm. This chemical shift is typical of phosphovanadomolybdate structures where the phosphorus heteroatom occupies only one position at the center of a Keggin structure [17]. Upon dehydration of the sample at 200 °C no change in the spectrum is observed. Heating the sample to 350 °C results in peak broadening and the appearance of new resonances. The formation of new signals over the range δ 5.0 ppm to δ −15.0 ppm is indicative of the solid undergoing major local structural changes on a molecular level. Further heating to 420 °C (the catalyst activation temperature prior to reaction) gives a spectrum similar to that obtained at 350 °C with some sharpening of resonances. The sharp signals at δ 3.0 ppm and δ −12.5 ppm occur where respectively "free phosphate" [18] and molybdenyl pyrophosphate $(MoO_2)_2P_2O_7$ [19] have previously been found.

After heating $NbPMo_{11}$Vpyr to 420 °C, the catalyst was exposed to ambient atmosphere for 48 h (Fig. 4). ^{31}P MAS NMR analysis of the sample showed the restoration of a single resonance at δ −3.6 ppm, strongly suggesting that the original Keggin structure has been reformed. Postactivation exposure to either dry air or oxygen-free water showed that the Keggin structure was reformed only in the presence of water. The small difference in chemical shift of the restored peak from the original peak may be attributed to the presence of water and the absence of pyridine. The weak shoulder upfield of the main resonance can be assigned to a Keggin structure with a different degree of hydration. Restoration of heteropolyanion structures via rehydration is consistent with previous reports [17]. This solid is not catalytically active.

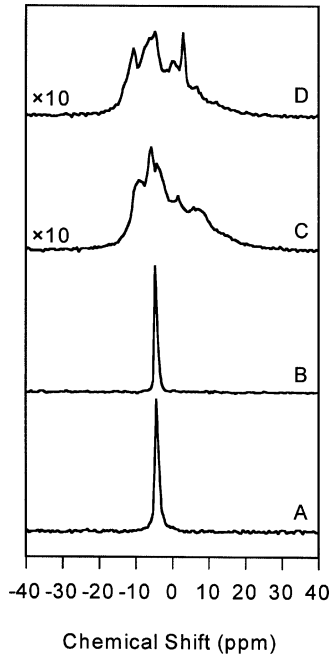

Fig. 3. ^{31}P MAS NMR spectra of $NbPMo_{11}$Vpyr heated to A = 30 °C, B = 200 °C, C = 350 °C, and D = 420 °C under helium. Spectra were recorded at room temperature.

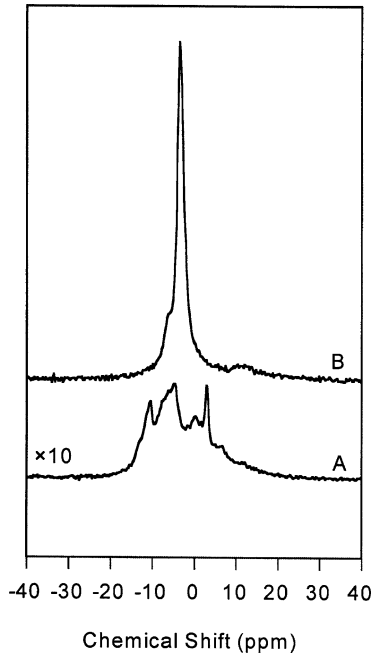

Fig. 4. ^{31}P MAS NMR spectra of $NbPMo_{11}$Vpyr heated to A = 420 °C and B = rehydrated in ambient atmosphere.

3.3. X-ray powder diffraction

In situ powder X-ray diffraction was performed on $PMo_{11}V$, $NbPMo_{11}V$, and $NbPMo_{11}Vpyr$ using heat treatments to 500 °C under flowing helium in an environmental chamber. The diffraction patterns obtained are given in Figs. 5–7. Crystalline phases have been assigned by comparison to those in the literature [20].

Phosphovanadomolybdic acid exists in a tetragonal arrangement (the so-called "anhydride" phase [20,21]) at room temperature and is stable to around 430 °C, where the phosphomolybdate is transformed into orthorhombic molybdenum trioxide (MoO_3) as shown in Fig. 5. Ion exchange of phosphovanadomolybdic acid with niobium gives $NbPMo_{11}V$ that has a cubic structure and is thermally stable to over 500 °C (Fig. 6). The inclusion of both niobium and pyridinium countercations and occluded pyridine in the secondary structure of the polyoxometalate strongly influences the crystal packing of $NbPMo_{11}pyr$ (Fig. 7). At room temperature the XRD pattern indicates that the solid is composed of heteropolyanion units organized in a mixture of triclinic and tetragonal crystalline phases. Heat treatment causes significant line broadening and some loss of intensity indicative of a partial loss of crystallinity. By 420 °C the solid is mostly amorphous except for a broad reflection at low angle ($2\theta = 9°$; $d = 10$ Å) that remains throughout the activation.

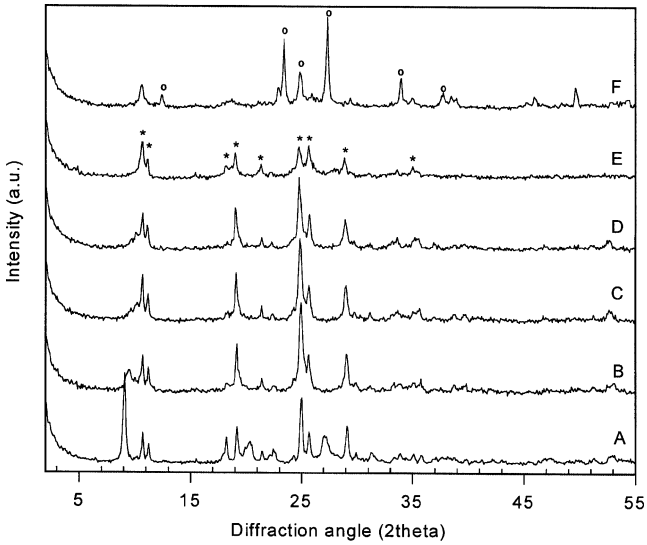

Fig. 5. In situ powder X-ray diffraction patterns of $PMo_{11}V$ during thermal treatment at A = 30 °C, B = 100 °C, C = 200 °C, D = 300 °C, E = 420 °C, F = 500 °C under flowing helium; tetragonal "anhydride" phase (∗) and orthorhombic MoO_3 (∘).

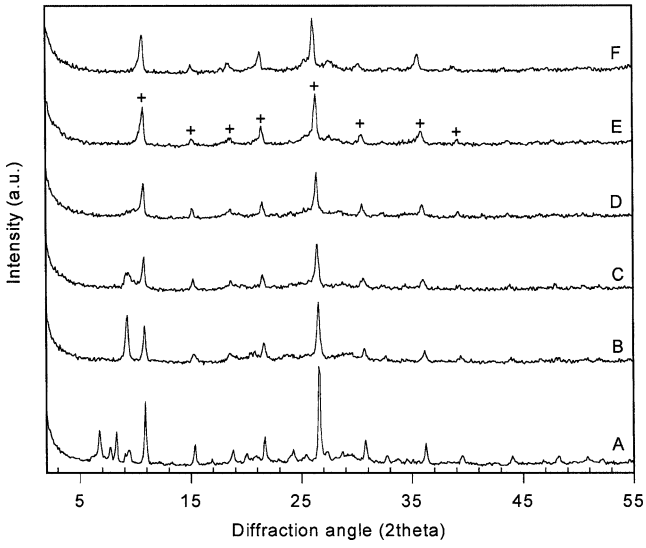

Fig. 6. In situ powder X-ray diffraction patterns of $NbPMo_{11}V$ during thermal treatment at A = 30 °C, B = 100 °C, C = 200 °C, D = 300 °C, E = 420 °C, F = 500 °C under flowing helium; cubic phase (+).

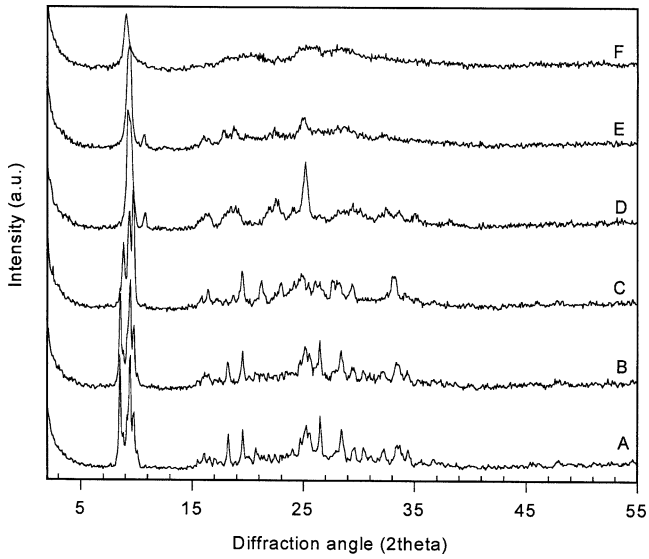

Fig. 7. In situ powder X-ray diffraction patterns of $NbPMo_{11}Vpyr$ during thermal treatment at A = 30 °C, B = 100 °C, C = 200 °C, D = 300 °C, E = 420 °C, F = 500 °C under flowing helium.

3.4. X-ray absorption spectroscopy

Niobium K edge electronic spectra (XANES) for niobium (IV) oxide (NbO_2) and niobium (V) oxide (Nb_2O_5) are presented in Fig. 8. Clearly, the near-edge shape changes as a function of oxidation state (Nb^{4+}/Nb^{5+}); this allows observation of discernable changes in the average oxidation state of niobium. Fig. 9 shows the niobium near-edge electronic spectra for $NbPMo_{11}Vpyr$ at a range of temperatures and under butane oxidation conditions. Changes in the near-edge shape are more visible in Fig. 9b. At room temperature and 200 °C the edge shape is characteristic of niobium in a +5 oxidation state. A shoulder approximately 15 eV above the edge becomes more evident as the temperature is increased to 420 °C causing the spectrum to resemble that of NbO_2 (niobium in a 4+ oxidation state). Exposure of the catalyst to reaction conditions produces an overall reduction in the magnitude of the white line while retaining the shape of the peak.

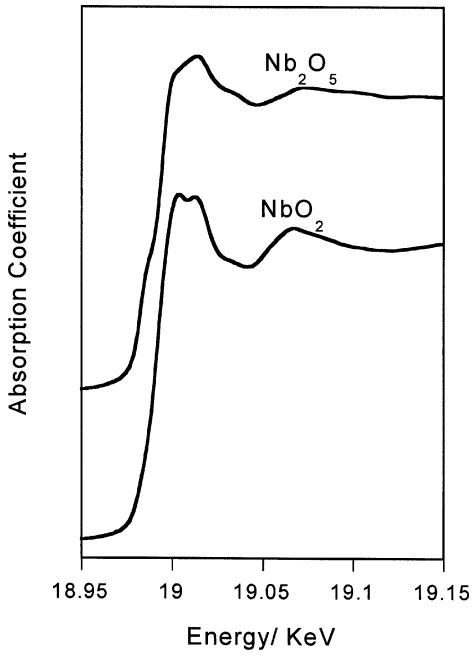

Fig. 8. Niobium K-edge spectra for Nb_2O_5 and NbO_2 as Nb^{5+} and Nb^{4+} standards, respectively.

The k^3-weighted EXAFS function associated with the Nb K edge of $NbMo_{11}Vpyr$ at 420 °C in helium is illustrated in Fig. 10a. The radial structure function in Fig. 10b shows major peaks at about 1.5 Å associated with backscattering from O neighbors and a peak at 3 Å most likely representing a Nb–Mo interaction. Each contribution to the Fourier transform was isolated by backtransforming over the region of interest. A niobium (II) oxide (NbO) standard was used with a first Nb–O shell distance of 2.105 Å and a coordination number of 4, and a second Nb–Nb shell at 2.977 Å and a coordination number of 8 [16]. Single-shell curve fits for Nb–O and Nb–Mo are shown in Figs. 10c and 10d, respectively. The structural parameters derived from the fits are summarized in Table 2.

Fig. 11 presents the radial structure functions derived from EXAFS associated with niobium K edge of $NbPMo_{11}Vpyr$ during heating to 420 °C and under reaction conditions. Peaks observed between 1 and 2 Å arise due to backscattering from oxygen atoms occupying first-neighbor positions to niobium. A peak at around 3 Å becomes evident at 350 °C and increases in magnitude at 420 °C and under reaction conditions. The peak occurs at a similar distance to Mo–O–Mo interactions observed in the Keggin unit (vide infra $NbPMo_{11}Vpyr$; Fig. 15). The radial structure plot for $(VO)PMo_{11}Nbpyr$ at room temperature and 420 °C is given in Fig. 12 for the niobium K edge, and is compared to that of $NbPMo_{11}Vpyr$ under similar conditions. At room temperature, a large peak at around 3 Å is observed for $(VO)PMo_{11}Nbpyr$ (solid line) that is absent for $NbPMo_{11}Vpyr$ (dashed line); this strongly suggests that niobium is occupying an addendum position in the framework of $(VO)PMo_{11}Nbpyr$ (to the authors' knowledge this observation is unprecedented in the literature), and an exchange position in $NbPMo_{11}Vpyr$. At 420 °C the data sets are very similar. Table 2 gives the structural parameters derived from fitting the data.

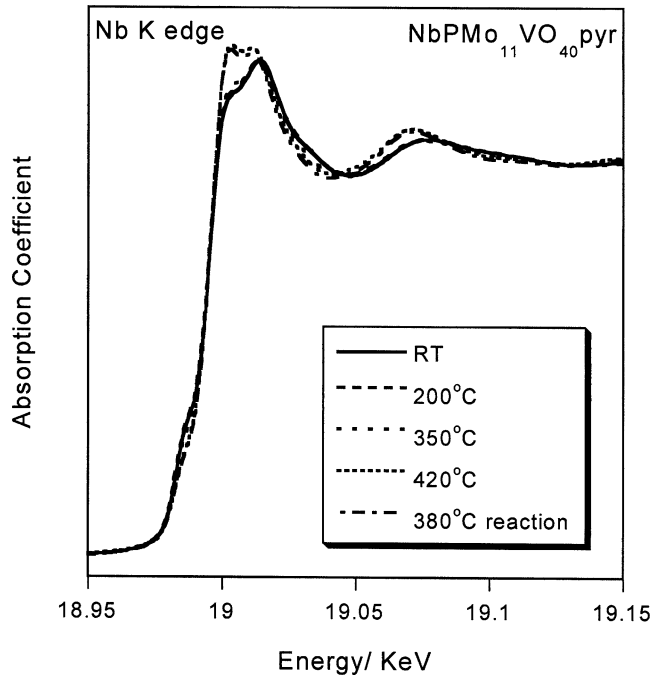

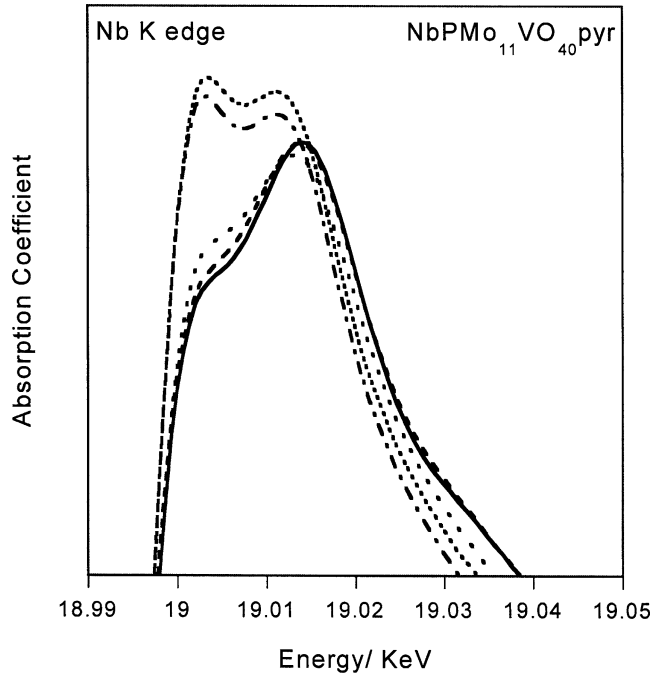

Fig. 9. (a) Niobium K-edge spectra for $NbPMo_{11}Vpyr$ as a function of temperature and atmosphere. (b) Enlarged niobium K-edge spectra for $NbPMo_{11}Vpyr$ as a function of temperature and atmosphere.

Molybdenum K-edge XANES for $NbPMo_{11}Vpyr$ (Mo^{6+}) and molybdenum (IV) oxide (Mo^{4+}) are given in Fig. 13.

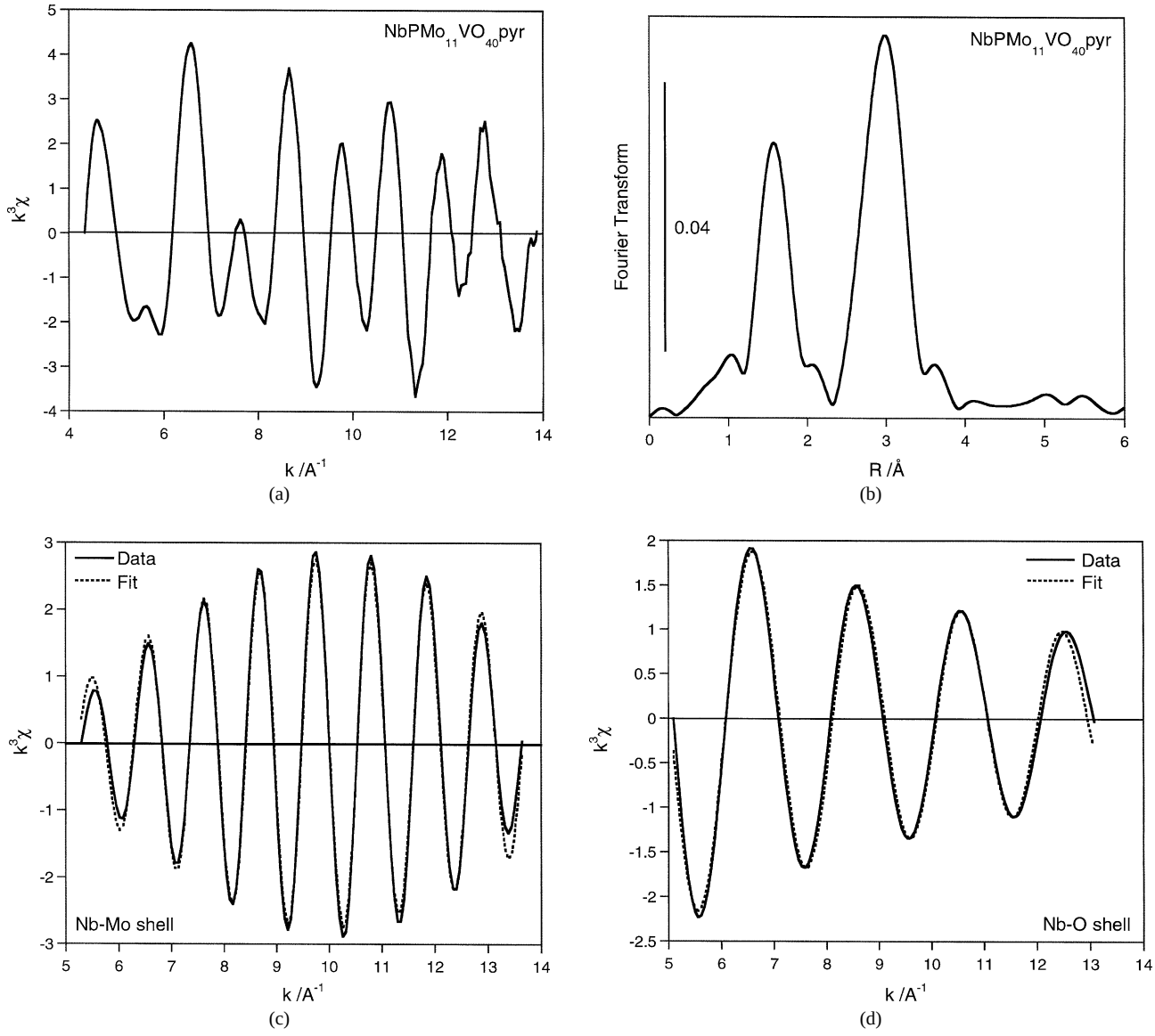

Fig. 10. (a) Niobium K-edge EXAFS for $NbPMo_{11}Vpyr$ at 420 °C in flowing helium. (b) Radial structure function (not corrected for phase shifts) derived from the Fourier transform of the niobium K-edge EXAFS for $NbPMo_{11}Vpyr$ at 420 °C in flowing helium. (c) Fourier-filtered EXAFS function of the Nb–O shell and resulting curve fit for $NbPMo_{11}Vpyr$ at 420 °C in flowing helium. (d) Fourier-filtered EXAFS function of the Nb–Nb shell and resulting curve fit for $NbPMo_{11}Vpyr$ at 420 °C in flowing helium.

Subtle changes in the shape of the near-edge spectra offer information regarding the average oxidation state of molybdenum in the sample. XANES was measured for $NbPMo_{11}Vpyr$ during activation to 420 °C and under reaction conditions while observing closely the molybdenum edge (Fig. 14). Changes in the near-edge features are observed around the shoulder at approximately 20 and 30 eV above the edge over this temperature range and under reaction conditions; these changes are more noticeable in Fig. 14b and suggest a change in the overall oxidation state of the molybdenum species in the catalyst.

The radial distribution functions of $NbPMo_{11}Vpyr$ during heat treatment and under catalytic conditions are given in Fig. 15. The peaks over the range 1 to 2.5 Å are associated with the Mo–O shell. At around 3 Å a peak suggestive of Mo–Mo interaction is shown to decrease in magnitude during exposure to higher temperatures. For molybdenum data fitting, a molybdenum (IV) sulfide (MoS_2) standard was used that has a first Mo–Mo shell at 3.15 Å and a coordination number of 6 [15]. Table 2 details the structural parameters.

3.5. *X-ray photoelectron spectroscopy*

The bulk elemental compositions of PMo_{12}, $NbPMo_{12}$, and $NbPMo_{12}pyr$ are given in Table 1. The surface elemental composition of the as-made samples at room temperature and after heating to 420 °C were determined by XPS curve fitting of the P (2p), Mo (3d 5/2) and Nb (3d 5/2) peaks.

Table 2
EXAFS fitting results for $NbPMo_{11}Vpyr$ and $(VO)PMo_{11}$ Nbpyr catalysts

Sample	Conditions	Absorber	Backscatterer	N^a	R^b (Å)	$\Delta\sigma^{2c}$ (Å^2)	$\Delta E_0{}^d$ (eV)
$NbPMo_{11}Vpyr$	25 °C	Nb	O	3.5	2.07	0.0043	5.0
	420 °C	Nb	O	3.8	2.04	0.0029	−7.0
	Reaction	Nb	O	4.8	2.10	0.0042	2.8
	25 °C	Nb	Mo	–	–	–	–
	420 °C	Nb	Mo	4.0	3.34	0.0010	−0.5
	Reaction	Nb	Mo	4.5	3.35	0.0007	1.1
	25 °C	Mo	Mo	4.0	3.45	0.0018	−2.6
	420 °C	Mo	Mo	2.5	3.49	0.0049	9.3
	Reaction	Mo	Mo	3.0	3.48	0.0054	7.6
$(VO)PMo_{11}$Nbpyr	25 °C	Nb	O	3.8	2.01	0.0001	8.5
	420 °C	Nb	O	4.7	2.11	0.0077	4.3
	Reaction	Nb	O	6.6	2.09	0.0103	2.0
	25 °C	Nb	Mo	3.9	3.46	0.0007	−2.7
	420 °C	Nb	Mo	3.2	3.34	0.0013	−2.5
	Reaction	Nb	Mo	3.2	3.33	0.0007	−1.7

[a] Coordination number.
[b] Interatomic distance.
[c] Change in Debye–Waller factor.
[d] Shift in edge energy required to optimize curve fit.

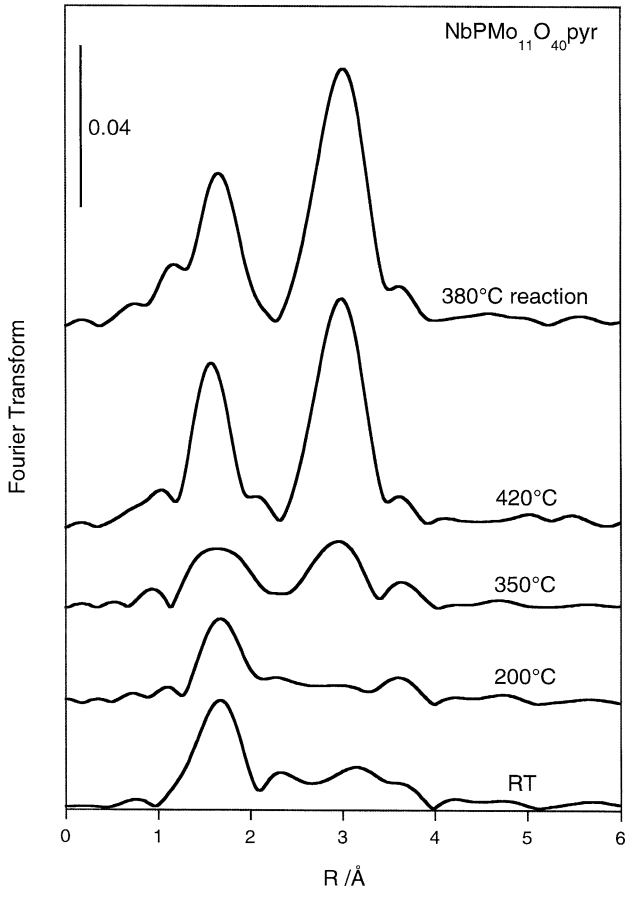

Fig. 11. Radial structure function (not corrected for phase shifts) derived from the Fourier transform of the niobium K-edge EXAFS for $NbPMo_{11}Vpyr$ as a function of temperature and atmosphere.

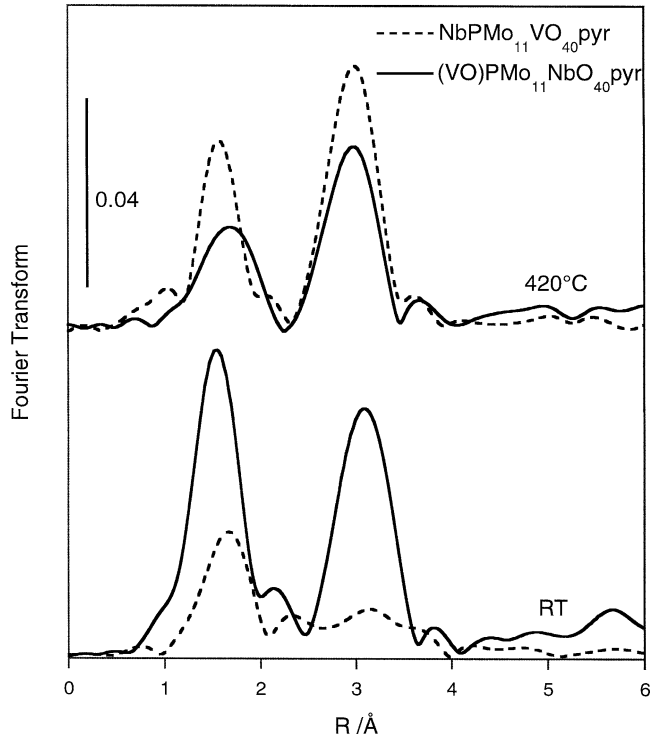

Fig. 12. A comparison of the radial structure functions (not corrected for phase shifts) derived from the Fourier transform of the niobium K-edge EXAFS for $(VO)PMo_{11}$Nbpyr and $NbPMo_{11}Vpyr$ at room temperature and at 420 °C.

A Mo/P ratio of around 9 is observed by XPS rather than 12 as expected for all as-made samples (Table 1). This may be explained by attenuation of the P (2p) signal from the surrounding 12 molybdenum octahedra. Indeed, simulation of the signal attenuation expected for MoO_6 surrounding a

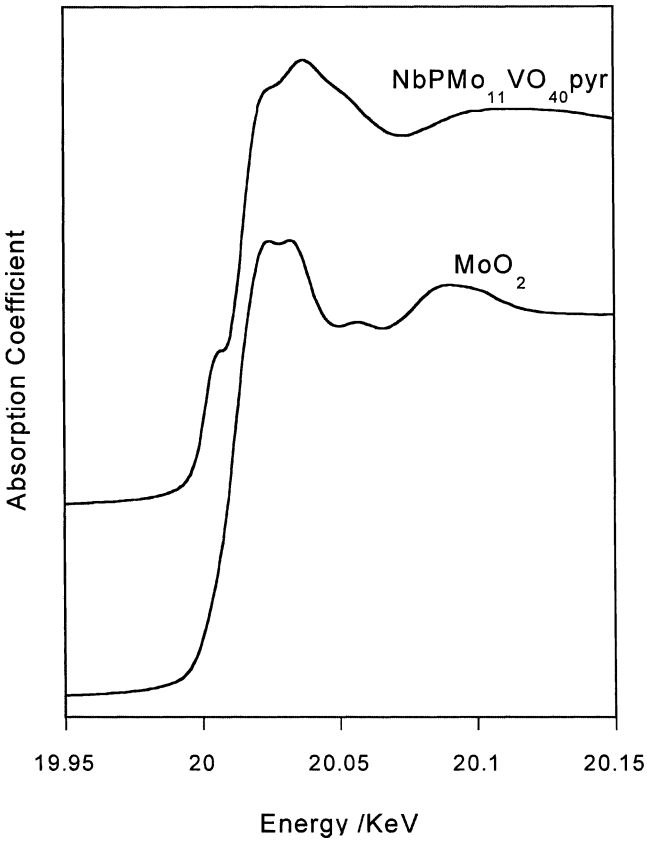

Fig. 13. Molybdenum K-edge spectra for $NbPMo_{11}Vpyr$ and MoO_2 as Mo^{6+} and Mo^{4+} standards.

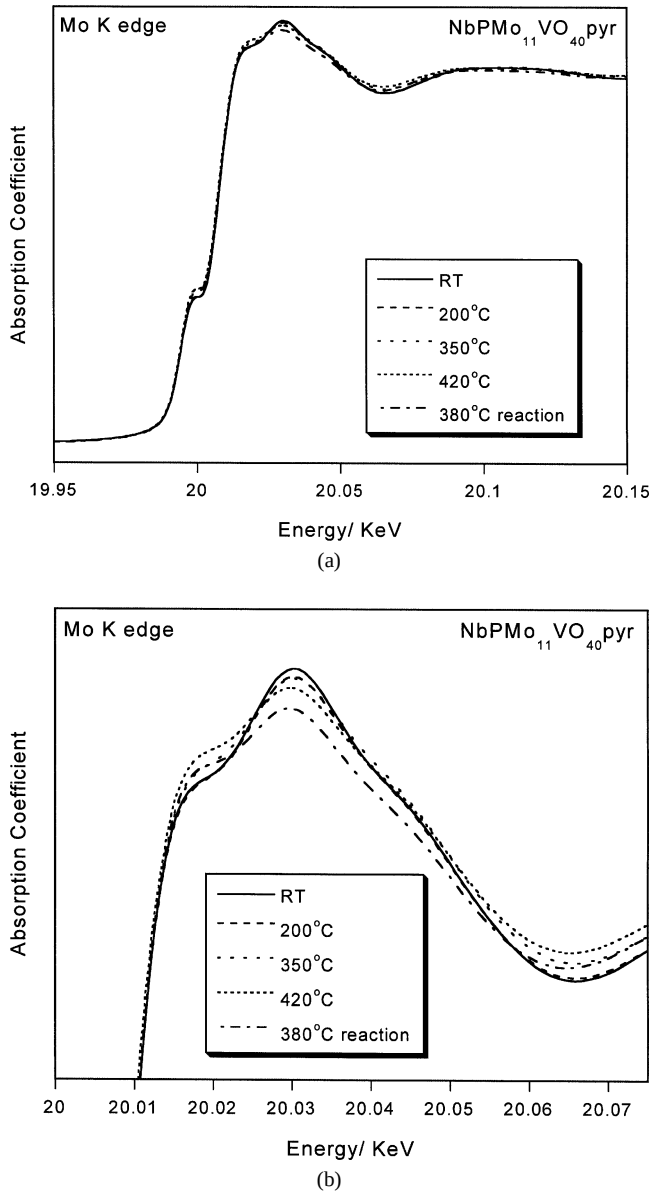

Fig. 14. (a) Molybdenum K-edge spectra for $NbPMo_{11}Vpyr$ as a function of temperature and atmosphere. (b) Enlarged molybdenum K-edge spectra for $NbPMo_{11}Vpyr$ as a function of temperature and atmosphere to show subtle changes.

phosphorus atom yields a Mo/P ratio of ∼9.4 (assuming a molybdenum layer thickness of ∼3.6 Å and a mean free path for the P (2p) photoelectron of ∼15 Å) supporting this proposal. This is consistent with observations in the literature [22,23]. Heating to 420 °C causes an increase in the P/Mo ratio at the surface for all catalysts, the effect being most evident for the heteropolyacid PMo_{12} and least for $NbPMo_{12}pyr$. For $NbPMo_{12}$ the surface and bulk Nb/Mo ratio are similar in the as-made catalyst and the ratio remains unchanged after activation to 420 °C. For as-made $NbPMo_{12}pyr$, the bulk Nb/Mo ratio was considerably higher at the surface than in the bulk; this may signify surface enrichment of niobium. The Nb/Mo ratio dropped after activation, possibly indicating depletion of niobium at the surface.

The binding energies and surface concentrations for phosphorus, molybdenum and niobium are listed in Table 3 for as-made and activated catalysts. The P (2p) binding energy corresponds to phosphorus in a +5 oxidation state and is unaffected by heat treatment. XPS of Mo (3d) in PMo_{12} shows that almost all the molybdenum in the as-made catalyst is in the +6 oxidation state (232.8–232.9 eV). Addition of niobium to the catalyst increases the amount of Mo^{5+} present (231.5–231.9 eV), likely because of the reducing capability of oxalic acid used as a precursor during the preparation of niobium containing catalysts. The binding energy of niobium itself (207.0–207.5 eV) corresponds to the +5 oxidation state. Upon addition of pyridine, Nb^{5+} is unaffected whereas Mo^{5+} is partially reoxidized to Mo^{6+} relative to the $NbPMo_{12}$ catalyst which is consistent with previous work [24]. Activation of PMo_{12} and $NbPMo_{12}$ to 420 °C causes no significant alteration in the relative oxidation states of molybdenum (Mo^{6+}/Mo^{5+}) from their room temperature states. However, 58% of the molybdenum in $NbPMo_{12}pyr$ is reduced from +6 to +5 oxidation state upon activation (58% would correspond to 7 out of 12 molybdenum atoms); for the same catalyst the niobium electron binding energy increases by around 1.0 to 207.9 eV.

Table 3
Binding energies for the P (2p), Mo (3d 5/2), and Nb (3d 5/2) energy levels for as-made and activated catalysts

Catalyst	As-made			Activated to 420 °C		
	P (2p)	Mo (3d) (% relative intensity)	Nb (3d)	P (2p)	Mo(3d) (% relative intensity)	Nb (3d)
PMo_{12}	133.9	232.9 (94)	–	134.3	233.4 (82)	–
		231.5 (6)			231.5 (18)	
$NbPMo_{12}$	133.7	232.9 (70)	207.5	134.2	233.6 (60)	208.4
		231.9 (30)			232.2 (40)	
$NbPMo_{12}$pyr	133.9	232.8 (83)	207.0	134.0	233.6 (42)	207.9
		231.6 (17)			232.1 (58)	

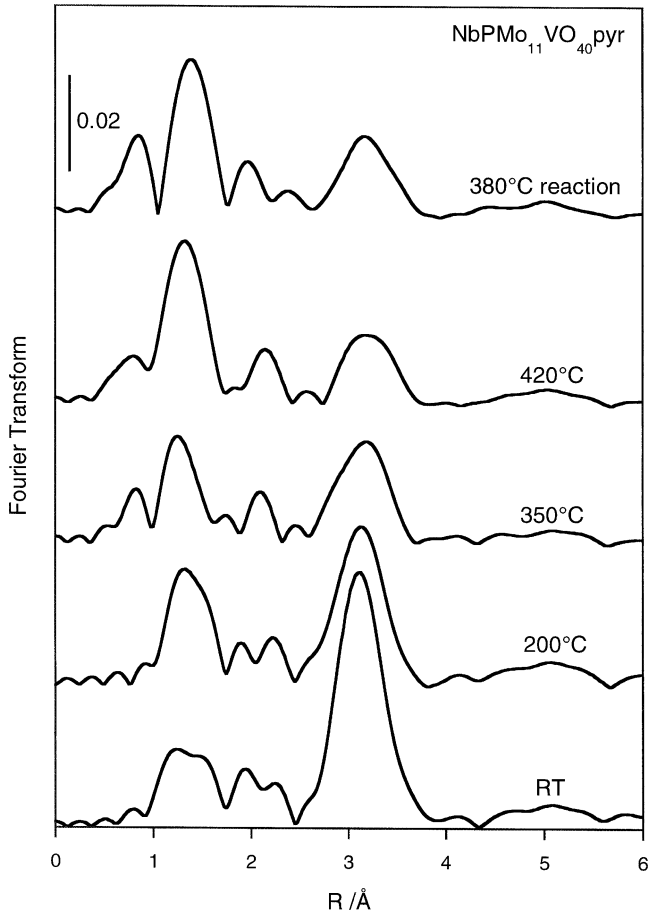

Fig. 15. Radial structure function (not corrected for phase shifts) derived from the Fourier transform of the molybdenum K-edge EXAFS for $NbPMo_{11}$Vpyr as a function of temperature and atmosphere.

4. Discussion

$NbPMo_{11}$Vpyr has been shown to be a substrate-versatile catalyst for the selective oxidation of light alkanes [13,25]. In order to achieve high activity and selectivity, $NbPMo_{11}$Vpyr must be pretreated by heating to 420 °C under a flowing inert atmosphere. Quantitative TGA–DSC analysis shows that the removal of pyridine occurs in two steps: occluded pyridine (C_5H_5N) desorbs over a low temperature range ($T < 300$ °C), while pyridinium species ($C_5H_5NH^+$)—more strongly bound to the phosphomolybdate through ionic bonding—desorb at higher temperatures (380–420 °C). Complete removal of pyridine species from the catalyst is achieved by 420 °C and is crucial for the catalyst to achieve an active state.

^{31}P MAS NMR and XRD measurements acquired during the activation process indicate that the loss of pyridinium from $NbPMo_{11}$Vpyr is accompanied by significant geometric changes of both the primary and secondary substructure of the solid (Figs. 3 and 7). Transformation of the single ^{31}P NMR resonance assigned to the central atom of the $PMo_{11}V$ Keggin heteropolyanion into several broad signals is observed at 350 and 420 °C. This observation strongly suggests primary Keggin ion structure alterations accompany removal of pyridine from the material. Possible changes in the Keggin unit suggested by the new ^{31}P NMR signals include ones such as the expulsion of a single octahedral metal atom from the framework (molybdenum or vanadium) to give a $PMo_{11}O_{39}^{7-}$-type structures whose ^{31}P NMR signal resonates at δ −1.5 ppm [19]; more extensive disintegration of the phosphorus local environment would result in the generation of mobile molybdenum oxide fragments and phosphate ions that have the ability to migrate, restructure, and reorganize to structures such as $PMo_9O_{31}^{6-}$ (δ −1.7 ppm), $PMo_{12}O_{40}^{3-}$ (δ −3.7 ppm), and $P_2Mo_{18}O_{62}^{6-}$ (δ −3.0 ppm). The species referred to above resonate close to where the broad signals are observed in Fig. 3; however, it is not our intention to assign these broad signals, but only to suggest that these and/or related species may form during activation of $NbPMo_{11}$Vpyr. The partial heteropolyanion structures are stable in the absence of pyridine; however, the Keggin ion is reformed upon exposure to water, indicating that no highly stable new phases are generated by activation (Fig. 4).

Comparison of the powder XRD data for $PMo_{11}V$, $NbPMo_{11}V$, and $NbPMo_{11}$Vpyr (Figs. 5–7) acquired at room temperature and 420 °C (catalyst activation temperature) illustrates the flexibility of the heteropolyanion secondary structure and its dependence on the presence and nature of countercations and additional occluded molecules. Dehydration of $PMo_{11}V$ results in the clear formation of the tetragonal “anhydride” structure (Fig. 5). At 420 °C a mixture of the anhydride phase and small amounts of a cubic phase are observed. It has been suggested that this cubic phase is the vanadyl salt of the heteropolyacid caused by ex-

pulsion of vanadium from the framework of $PMo_{11}V$ [21]. This material is not catalytically active for the oxidation of propane and butane under the conditions used here. The cubic structure that is formed by addition of niobium as countercation in $NbPMo_{11}V$ (Fig. 6) is isomorphous with the vanadyl salt of PMo_{12}. Indeed, the presence of alkali metals as countercations has been found to cause the heteropolyanions to arrange in a similar cubic phase, which is strongly related to catalytic inactivity for oxidation reactions [12]. Once pyridine is introduced to give $NbPMo_{11}Vpyr$, the polyoxometalate becomes a complex mixture of triclinic and tetragonal phases (Fig. 7) as a result of the replacement of crystalline water by pyridine and the presence of *both* niobium and pyridinium as countercations. The pyridine species desorb through heat treatment and at 420 °C the mostly amorphous nature of the XRD pattern is indicative of significant disorder. The broad feature that remains through activation at around $2\theta = 9°$ ($d = 10$ Å) is certainly evidence of some remaining long-range order which may represent remaining secondary structure from the Keggin unit packing. Considering that the solid may comprise several varieties of defective heteropolyanions according to ^{31}P NMR, the absence of long-range order in the material is not surprising.

The 5+ and 4+ oxidation states of niobium are easily distinguishable in the XAS spectrum at the K edge. For Nb^{5+} the edge structure shows a single peak with a shoulder, while Nb^{4+} exhibits two peaks (Fig. 8). Hence, in addition to the expected shifts in edge energy associated with changes in the oxidation state, niobium exhibits a modified near-edge structure that allows subtle changes in oxidation state to be observed that are beyond the energy resolution of the monochromator.

XANES of $NbPMo_{11}Vpyr$ during activation reveals changes in the oxidation state of niobium as a function of pretreatment temperature (Figs. 9a and 9b). Small changes in edge shape are observed between room temperature and 350 °C, whereas between 350 and 420 °C significant changes occur. TGA–DSC analysis indicated that pyridinium species are lost over this temperature range. A linear combination XANES fit using Nb_2O_5 and NbO_2 standards suggests that all niobium in the catalyst is reduced from 5+ to 4+ at 420 °C. No further change in the shape of the niobium K edge is observed by exposing the catalyst to the reaction mixture, although the magnitudes of the peaks decrease slightly. These observations imply that pyridinium acts as an in situ reductant during catalyst activation to 420 °C. The composition of the reaction mixture is sufficiently nonoxidizing to maintain the reduced state of niobium. XANES of $(VO)PMo_{11}Nbpyr$ (data not shown) is very similar to $NbPMo_{11}Vpyr$, indicating that the redox behavior of niobium is independent of its initial position (countercation or addenda atom) in the as-made catalyst.

EXAFS associated with the Nb K edge provides information on the local structure of niobium in the polyoxometalate. At room temperature, $NbPMo_{11}Vpyr$ exhibits features below 2 Å indicative of a niobium–oxygen interaction (Fig. 11). A distance of 2.07 Å and a coordination number of 3.5 is found through fitting (Table 2). Additional interactions at larger distances are of low magnitude. This is consistent with a niobyl species occupying a countercation position. Although heating from room temperature to 420 °C in an inert atmosphere caused no change in the Nb–O coordination number and a slight decrease in the interatomic distance, introduction of the reaction mixture brought about an increase in both parameters. A structural change associated with the first-neighbor shell (oxygen) only under reaction conditions is not unexpected since there is molecular oxygen present in the reactant feed [26].

EXAFS of $(VO)PMo_{11}Nbpyr$ at room temperature indicates that the coordination number of niobium to oxygen is 4 (Table 2). This is consistent with niobium occupying a framework position in the heteropolyanion that is clearly observed from the radial structure functions (Fig. 12) which show strong Nb–Mo interactions at 3.46 Å (close to the Mo–Mo distance of 3.45 Å). A Nb–O interatomic distance of 2.01 Å is observed. An average distance of 1.99 Å has been calculated for Mo–O distances in Keggin heteropolymolybdates [9]. The coordination number and interatomic distance of niobium with respect to oxygen during heat treatment to 420 °C is similar for both $(VO)PMo_{11}Nbpyr$ and $NbPMo_{11}Vpyr$ catalysts; this illustrates that the position of niobium in the active phase is independent of the initial position of niobium in the as-made catalyst, be it exchange cation or addenda atom. This is further evidenced by comparison of the radial structure functions of both $(VO)PMo_{11}Nbpyr$ and $NbPMo_{11}Vpyr$ at 420 °C in Fig. 12.

During heating from 350 to 420 °C, a significant increase in the intensity of the interaction around 3 Å is observed in niobium EXAFS for $NbPMo_{11}Vpyr$ (Fig. 11). It is assumed that this second-neighbor shell is composed mostly of molybdenum, considering average metal–metal distances and the stoichiometry of metals in the polyoxometalate (Nb:Mo:V $\approx$ 1:44:1). Data fitting indicates that the coordination number of niobium to molybdenum is 4 with an interatomic distance of 3.34 Å.

At 420 °C, EXAFS suggests the local structure of niobium in both $(VO)PMo_{11}Nbpyr$ and $NbPMo_{11}Vpyr$ catalysts are very similar; niobium is coordinated to 3 or 4 molybdenum neighbors at distances of 3.34 Å (Fig. 12 and Table 1). It is unlikely that niobium is located in an intact Keggin ion considering that a 3.46 Å Nb–O–Mo distance is observed for niobium in an addenda position of a Keggin unit prior to activation (0.1 Å longer than the Nb–O–Mo distance observed after activation). In addition, there are concomitant increases in Nb–O coordination numbers and interatomic distances during activation. Overall comparison of both Nb–O and Nb–O–Mo structural features in activated and as-made $(VO)PMo_{11}Nbpyr$ and $NbPMo_{11}Vpyr$ catalysts strongly suggests the combination of niobium oxo-species with heteropolymolybdate fragments. Ternary mixed oxides of niobium, molybdenum and other metals are known; niobium and molybdenum, atoms are configured in

octahedral arrangements bound to one another through oxygen bridges [27]. Although the typical Nb–O coordination number reported here is approximately 4, this value represents the major peak only. The presence of shoulders on the main peak at both shorter and longer distances at 420 °C and under reaction conditions visible in Fig. 10 indicates the coordination of additional oxygen atoms. Therefore, we propose that activated (VO)PMo_{11}Nbpyr and $NbPMo_{11}$Vpyr catalysts form an active phase of small metal oxide clusters made up of edge-bound distorted octahedra. Corner-sharing octahedra would require M–O–M distances being twice the M–O distance; this is not observed in our measurements. Identification of this phase is difficult; however, octahedra of the type found in MoO_2, MoO_3, NbO_2, or Nb_2O_5 bulk oxides can be excluded on the basis of the derived structural parameters. Several other niobium–oxygen surface clusters are known; based on fitting analysis these structures are also inconsistent with our system [28,29]. The structural parameters of a niobate-type structure $Nb_6O_{19}^{8-}$ (metal–metal distance of 3.36 Å and coordination number of 4) show some similarity to the calculated parameters of our active phase [30].

XANES of $NbPMo_{11}$Vpyr during heat treatment shows changes in the Mo K-edge structure, indicative of a change in oxidation state (Figs. 14a and 14b). A linear combination fit suggests that one or two molybdenum atoms per Keggin unit undergo reduction from +6 to +5 oxidation state. During reaction the change in edge structure suggests partial reoxidation of molybdenum by gas-phase oxygen; this observation is consistent with the accepted catalytic cycle for selective oxidation [26]. As also indicated by XPS analysis for $NbPMo_{12}$pyr, molybdenum undergoes reduction from Mo^{6+} to Mo^{5+} during desorption of pyridine.

Relatively more Mo^{5+} than Mo^{6+} is identified by XPS than by XANES; this is likely a consequence of photoelectron spectroscopy analyzing only the catalyst surface and X-ray spectroscopy analyzing the bulk of the material. The higher degree of reduction (Mo^{5+}/Mo^{6+} ratio) observed at the surface of the activated catalyst is possibly a result of a pyridine concentration gradient across the catalyst with a higher concentration of the organic base at the surface. It has also been argued that partially reduced metal oxides may have an inherent preference for the surface to be more reduced than the bulk [31].

Evidence presented from XRD, ^{31}P NMR, EXAFS, and XPS strongly suggests structural rearrangement of the Keggin heteropolyanion during activation and reaction of the most active catalyst $NbPMo_{11}$Vpyr. A strong Mo–O–Mo interaction is observed at around 3 Å from EXAFS (Fig. 15) for $NbPMo_{11}$Vpyr; during the activation procedure to 420 °C, the intensity of this interaction is reduced considerably, reflecting a decrease in the number of molybdenum second nearest neighbor interactions in this range. In the activated state the average coordination number of molybdenum is decreased from 4 to around 2.5, implying that some molybdenum no longer occupies a framework atom position in a Keggin unit. In addition, XPS data indicate less molybdenum is associated with phosphorus at the surface of $NbPMo_{12}$pyr in the activated state.

XANES of niobium in $NbPMo_{12}$pyr reveals reduction to the +4 oxidation state during heating to 420 °C. Considering the increase in reactivity observed when niobium is present in these catalysts, it is highly likely that niobium participates in the oxidation–reduction cycle during selective alkane oxidation [13]. However, the reduction was not detected by XPS; the binding energy of niobium increased during activation by around 1 to 207.9 eV, rather than decreasing by a similar amount as would be expected for reduction to a +4 oxidation state. This apparent discrepancy may be rationalized in two ways: an effect of particle size and XPS final state effects. Binding energies used as references for oxidation states are generally recorded for bulk metal oxides with large particle sizes [32]. Binding energies measured for smaller particles are often higher because relaxation is inhibited by a lack of local electron density [33–35]. Our result is not unprecedented; the same discrepancy was previously observed in XPS and XAS analyses of niobium oxidation states (XPS indicated Nb^{5+} while XAS indicated Nb^{4+}). The authors rationalized their results by either the presence of small particles or contamination causing oxidation of the surface [36]. Higher than expected binding energies are also often observed as a result of final state effects. A final state effect is similar to a particle size effect in that it results from a lack of extra-atomic relaxation from the environment causing binding energy increases. We suggest that the active state of these niobium and pyridine containing phosphomolybdates is composed of small mixed metal oxide clusters composed mainly of molybdenum; an environment lacking in electron density may be created around these clusters considering that molybdenum is more electronegative than niobium. This environment may also reduce the ability of the niobium to electronically relax after excitation, resulting in a higher binding energy.

5. Conclusions

The loss of pyridinium species over the temperature range 380 to 420 °C (catalyst activation temperature) from $NbPMo_{12}$pyr- and $NbPMo_{11}$Vpyr-type polyoxometalates is accompanied by significant structural and electronic changes in the catalyst. During this activation period ^{31}P NMR results indicate that the heteropolyanion is transformed to produce several distinct phosphorus environments. Partial decomposition of the Keggin unit in this way results in the formation of mobile molybdenum–oxygen and niobium–oxygen fragments (oxoanions) that likely migrate and combine to form small mixed-metal oxide clusters. Due to the irregular shape and size of these clusters, and the irregular structure of the decomposed primary structure, no short range order is observed by in situ X-ray powder diffraction although a repeating unit of approximately 10 Å is observed. Af-

ter activation of both $NbPMo_{11}Vpyr$ and $(VO)PMo_{11}Nbpyr$, structures with similar Nb–O–Mo coordination numbers and identical interatomic distances are obtained and demonstrate the indifference of the active structure to initial niobium positioning. XPS and XANES analyses reveal that the charged pyridinium species reduce the molybdenum and niobium centers upon removal from the solid during activation. Reduction of Nb^{5+} to Nb^{4+} is observed by XANES, whereas some nonreduced molybdenum remained in the catalyst after activation with Mo^{5+}/Mo^{6+} ranging from 0.58 at the surface (XPS) to 0.17 in the bulk (XANES).

Acknowledgments

This research was carried out in part at the National Synchrotron Light Source, Brookhaven National Laboratory, which is supported by the US Department of Energy. G.W. Zajac and T. Nguyen (BP) are acknowledged for X-ray photoelectron spectroscopy experiments and useful discussions. This work was funded by BP.

References

[1] G. Centi, F. Cavani, F. Trifiro, Selective Oxidation by Heterogeneous Catalysis, Kluwer, New York, 2001.
[2] M.T. Pope, A. Müller (Eds.), Polyoxometalates: From Platonic Solids to Anti-Retroviral Activity, Kluwer, the Netherlands, 1994.
[3] K. Oshihara, T. Hisano, W. Ueda, Top. Catal. 15 (2001) 153.
[4] P. Botella, J.M. López Nieto, B. Solsona, Catal. Lett. 78 (2002) 383.
[5] P. Botella, J.M. López Nieto, B. Solsona, A. Mifsud, F. Márquez, J. Catal. 209 (2002) 445.
[6] T. Ushikubo, H. Nakamura, Y. Koyasu, S. Wajiki, Mitsubishi Kasei, US Patent 5,380,933, 1995.
[7] H. Tsuji, Y. Koyasu, J. Am. Chem. Soc. 124 (2002) 5608.
[8] M. Misono, Chem. Commun. (2001) 1141.
[9] T. Okuhara, N. Mizuno, M. Misono, Adv. Catal. 41 (1996) 113.
[10] N. Mizuno, D.-J. Suh, W. Han, T. Kudo, J. Mol. Catal. A 114 (1996) 309.
[11] E. Blouet-Crusson, M. Rigole, M. Fournier, A. Aboukais, F. Daubrege, G. Hecquet, M. Guelton, Appl. Catal. A 178 (1999) 69.
[12] W. Li, K. Oshihara, W. Ueda, Appl. Catal. A 182 (1999) 357.
[13] J.H. Holles, C.J. Dillon, J.A. Labinger, M.E. Davis, J. Catal., in press.
[14] T. Ressler, J. Phys. IV 7 (1997) C2.
[15] R.G. Dickenson, L. Pauling, J. Am. Chem. Soc. 45 (1923) 1466.
[16] A.L. Bowman, T.C. Wallace, J.L. Yarnell, R.G. Wenzel, Acta. Crystallogr. 21 (1996) 843.
[17] N. Essayem, Y. Tong, H. Jobic, J.C. Vedrine, Appl. Catal. A 194 (2000) 109.
[18] J.A.R. van Veen, O. Sudmeijer, C.A. Emeis, H. de Wit, J. Chem. Soc. Dalton Trans. (1986) 1825.
[19] R.I. Maksimovskaya, V.M. Bondareva, Russ. J. Inorg. Chem. 39 (1994) 1238.
[20] M. Fournier, C. Feumi-Janou, C. Rabia, G. Herve, S. Launay, J. Mater. Chem. 2 (1992) 971.
[21] T. Ilkenhans, B. Herzog, T. Braun, R. Schlögl, J. Catal. 153 (1995) 275.
[22] S. Damyanova, J.L.G. Fierro, I. Sobrados, J. Sanz, Langmuir 15 (1999) 469.
[23] M. Langpape, J.M.M. Millet, U.S. Ozkan, M. Boudeulle, J. Catal. 181 (1999) 80.
[24] W. Turek, E. Pomarzanska, A. Pron, J. Haber, J. Catal. 189 (2000) 297.
[25] M.E. Davis, C.J. Dillon, J.H. Holles, J.A. Labinger, Angew. Chem. 41 (2002) 858.
[26] P. Mars, D.W. van Krevelen, Chem. Eng. Sci. 3 (1954) 41.
[27] J.M.M. Millet, H. Roussel, A. Pigamo, J.L. Dubois, J.C. Jumas, Appl. Catal. A 232 (2002) 77.
[28] N. Ichikuni, Y. Iwasawa, J. Phys. Chem. 98 (1994) 11576.
[29] N. Ichikuni, M. Shirai, Y. Iwasawa, Catal. Today 28 (1996) 49.
[30] A. Goiffon, E. Philippot, M. Maurin, Rev. Chim. Miner. 17 (1980) 466.
[31] J.A. Labinger, K.C. Ott, Catal. Lett. 4 (1990) 245.
[32] D. Briggs, M.P. Seah (Eds.), Practical Surface Analysis: Auger and X-ray Photoelectron Spectroscopy, Wiley, New York, 1996.
[33] C.C. Chusuei, X. Lai, K. Luo, D.W. Goodman, Top. Catal. 14 (2001) 71.
[34] V. Vijayakrishnan, C.N.R. Rao, Surf. Sci. 225 (1991) L516.
[35] R.L. Chin, D.M. Hercules, J. Phys. Chem. 86 (1982) 360.
[36] J. Pollman, in: X-ray Photoelectron Spectroscopy of Transition Metal Colloids and Supported Catalysts, University of Bonn, Physikalisches Institut, Bonn, 1998, p. 1.